Plasmonic-enhanced catalytic activity of methanol oxidation on Au–graphene–Cu nanosandwiches

Yaxing Liu,[a,b] Fuyi Chen,*[a,b,c] Qiao Wang,[a,c] Junpeng Wang,[a,c] Jiali Wang,[a,c] Longfei Guo,[a,c] and Tesfaye Tadesse Gebremariam[c]

[a] State Key Laboratory of Solidification Processing, Northwestern Polytechnical University, Xi'an 710072, China

[b] School of Electronics and Information, Northwestern Polytechnical University, Xi'an 710072, China

[c] School of Materials Science and Engineering, Northwestern Polytechnical University, Xi'an 710072, China

***Corresponding author:**

Fuyi Chen
State Key Laboratory of Solidification Processing, Northwestern Polytechnical University, Xian, 710072, P. R. China
Email: fuyichen@nwpu.edu.cn

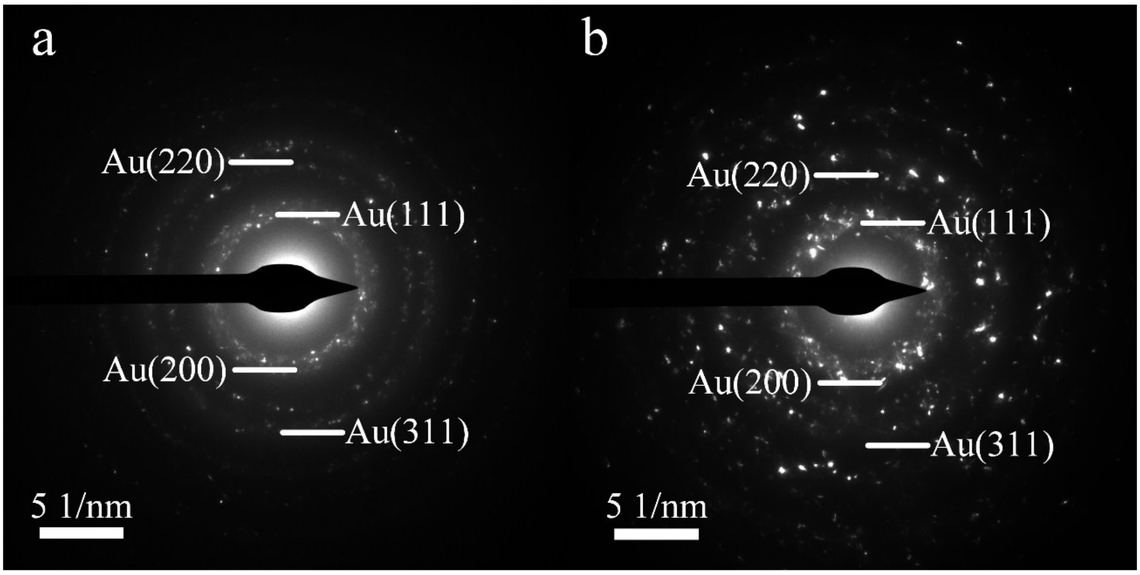

Figure S1 Selected-area electron diffraction pattern of AuNPs in (a) Au–3T/SG/Cu and (b) Au–10T/SG/Cu catalytic electrodes.

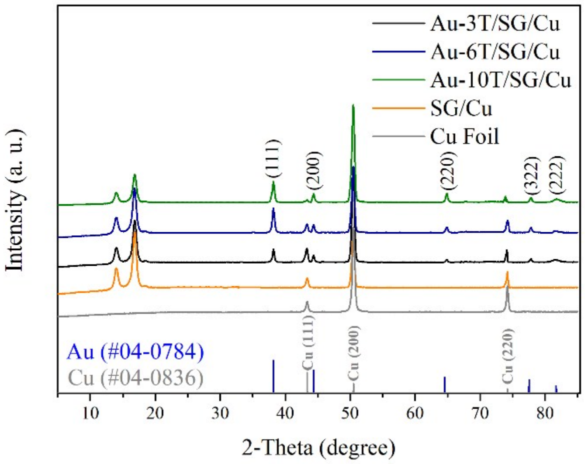

Figure S2 XRD patterns of Au–3T/SG/Cu, Au–6T/SG/Cu and Au–10T/SG/Cu catalytic electrodes compared with that of SG/Cu and Cu foil. The insets indicate the details of the corresponding diffraction peaks. Bar diagram: Au #04-0784 and Cu #04-0836.

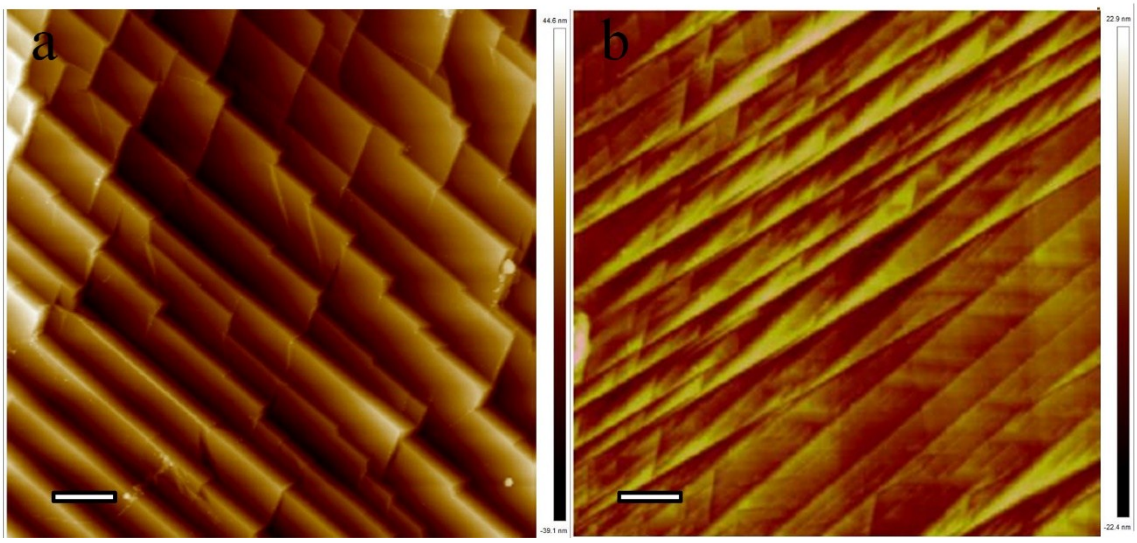

Figure S3 Tapping-mode AFM images of (a) Cu foil and (b) single-layer graphene on the Cu foil (SG/Cu) sample. (Scale bar of 200 nm).

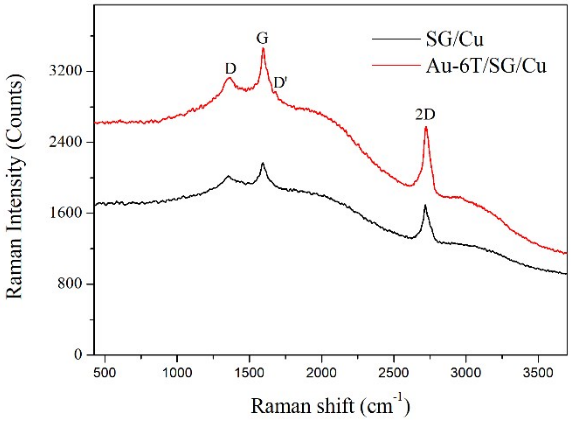

Figure S4 Raman spectra of the Au–6T/SG/Cu catalytic electrode and the SG/Cu sample.

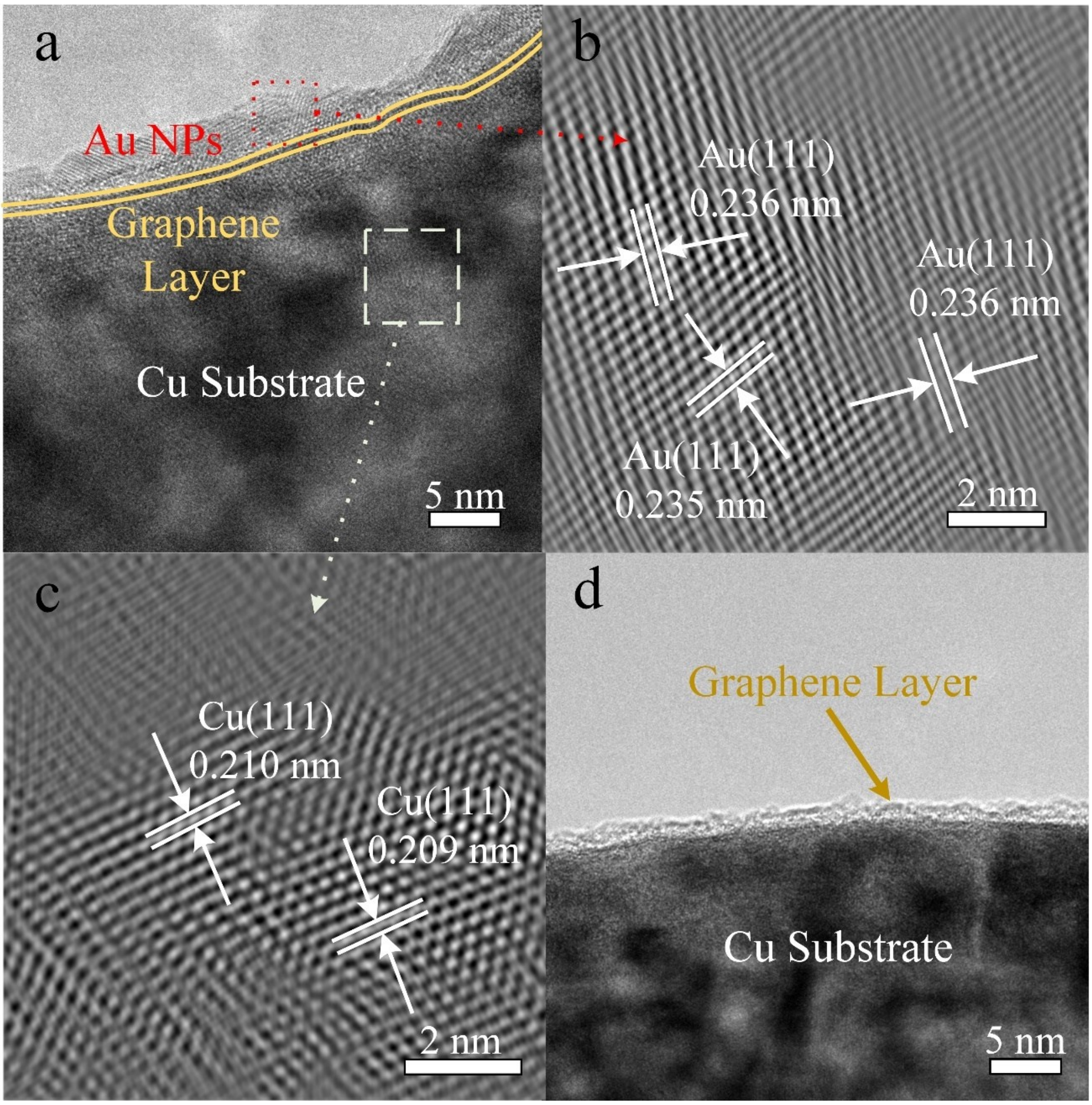

Figure S5 (a) Cross-sectional HR-TEM image of Au–6T/SG/Cu catalytic electrode. (b) and (c) IFFT images corresponding to the two selected areas in (a). (d) Cross-sectional HR-TEM image of SG/Cu sample.

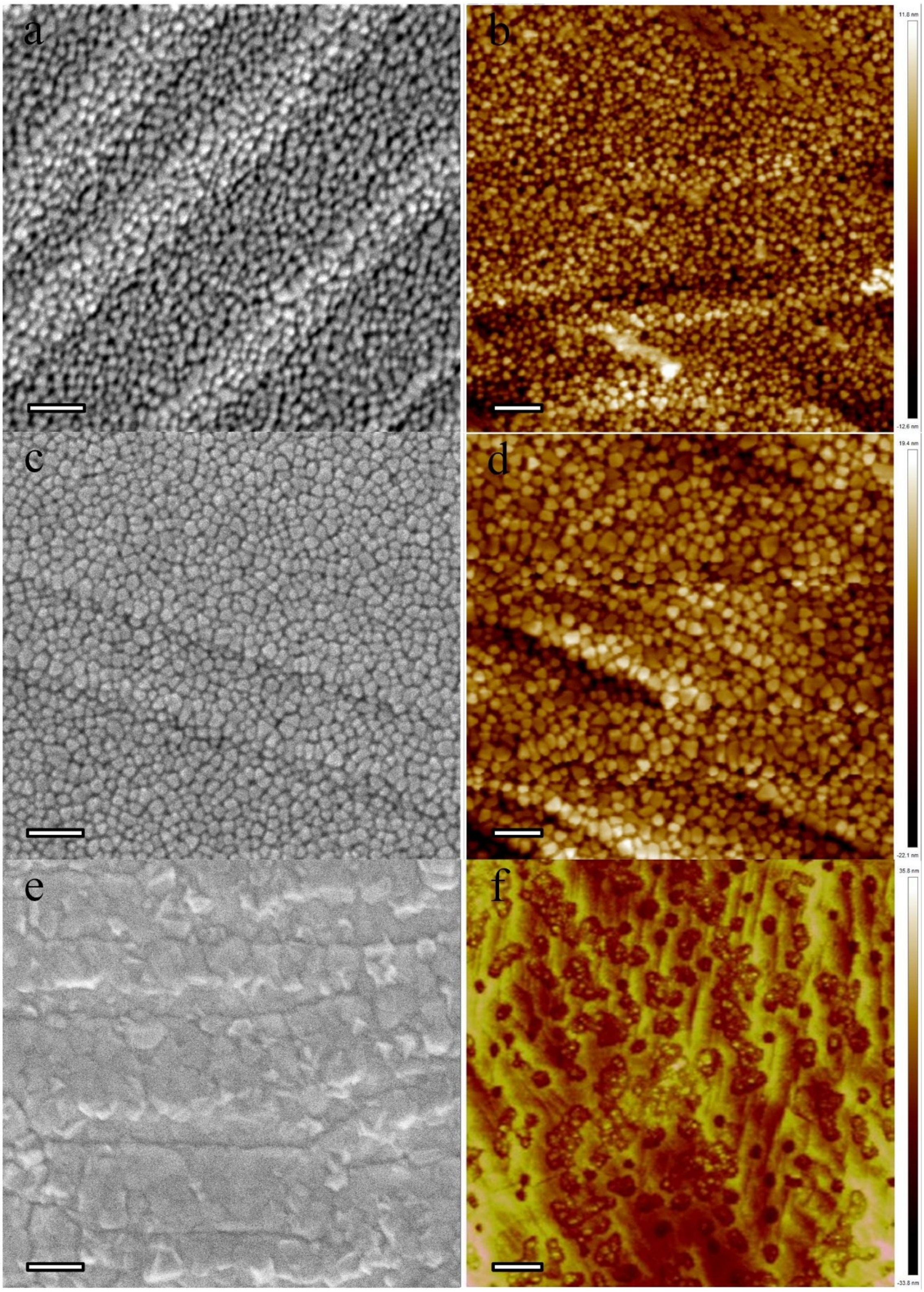

Figure S6 Morphology characterisations of Au–n/SG/Cu catalytic electrode. (a–c) FE-SEM and (a–e) tapping-mode AFM images of Au–3T/SG/Cu, Au–6T/SG/Cu and Au–10T/SG/Cu catalytic electrodes, respectively. (Scale bar of 100 nm).

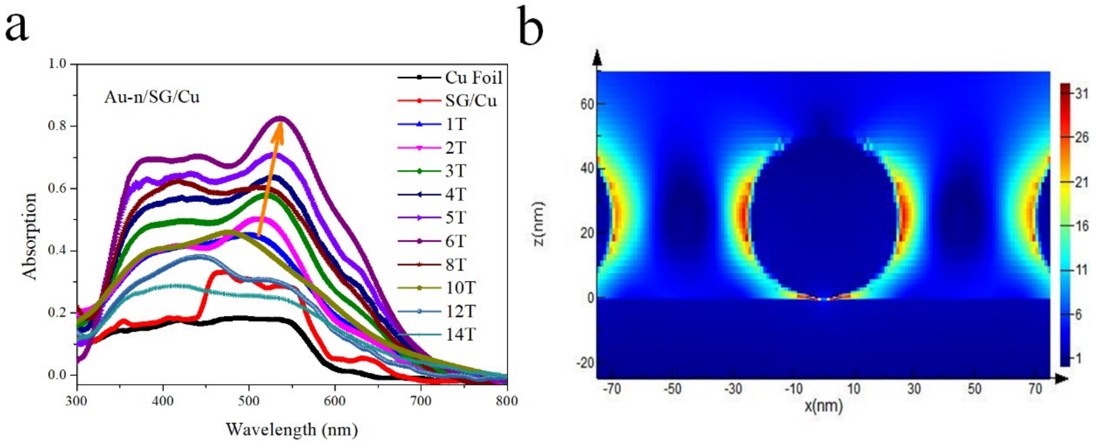

Figure S7 (a) Diffuse reflectance UV–vis absorption spectra of Cu foil, SG/Cu and Au–n/SG/Cu catalytic electrodes (n = 1T, 2T, 3T, 4T, 5T, 6T, 8T, 10T, 12T, 14T). (b) Cross-sectional plasmonic near-field distribution of Au–6T/SG/Cu catalytic electrode at excitation wavelength of 565 nm. The electrical field was investigated using FDTD method.

Table S1 Performance parameters of the photocurrent, the anodic peak current for MOR and the ratio of anodic peak current for MOR under light/dark.

Sample	Photocurrent	I_{MOR}		I_{Light}/I_{Dark}	References
		Dark	Light		
Au–6T/SG/Cu	303 (μA μg^{-1})	167 (μA μg^{-1})	288 (μA μg^{-1})	1.72	**This work**
Au NPs/GC	1.1 (μA)	0.65 (μA)	1.2 (μA)	1.85	1
Au DNFs	250 (μA)	0.95 (μA μg^{-1})	3.14 (μA μg^{-1})	3.3	2
Au/TiO_2	0.6 (mA cm^{-1})	0.61 (mA cm^{-1})	1.11 (mA cm^{-1})	1.82	3
Au-CA	215 (μA μg^{-1})	116 (μA μg^{-1})	249 (μA μg^{-1})	2.15	4
Au@TiO_2	--	--	5 (mA cm^{-1})	--	5
MWNT-g-PANI-Au	--	17 (μA cm^{-1})	--	--	6
Au/C	--	75 (mA mg^{-1})	--	--	7
Porous Au nanotubes	--	23 (μA μg^{-1})	--	--	8
np-Au	--	17.5 (μA μg^{-1})	--	--	9
$(Au/GO)_n$ multilayer	--	2.2 (mA cm^{-1})	--	--	10

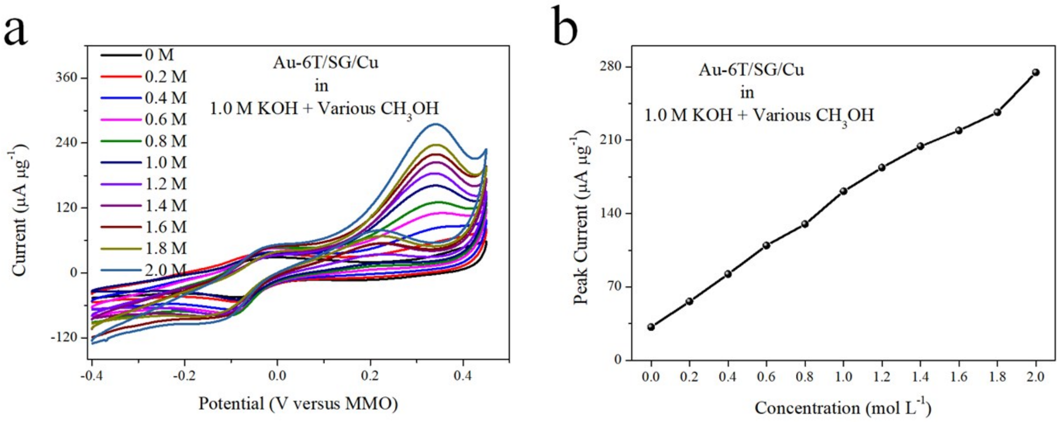

Figure S8 Effects of methanol concentrations on the methanol oxidation performance of Au–6T/SG/Cu catalytic electrode in a deoxygenated solution of 1.0 M KOH. (a) CV curves of Au–6T/SG/Cu catalytic electrode recorded at various methanol concentrations. (b) Anodic peak currents during methanol oxidation on Au–6T/SG/Cu catalytic electrode at various methanol concentrations.

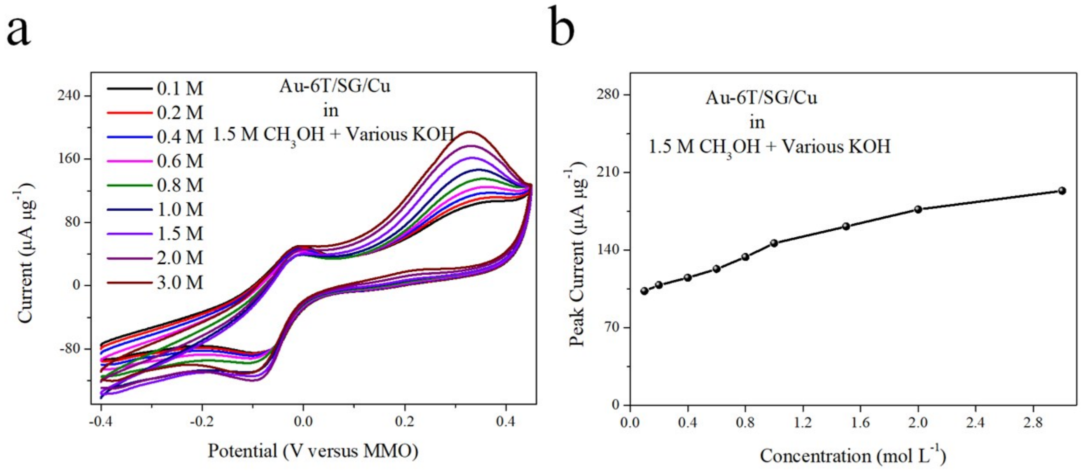

Figure S9 Effects of alkaline concentrations on the methanol oxidation performance of Au–6T/SG/Cu catalytic electrode. (a) CV curves of Au–6T/SG/Cu catalytic electrode recorded in a deoxygenated solution of various KOH concentrations mixed with 1.5 M CH_3OH. (b) Anodic peak currents during methanol oxidation on Au–6T/SG/Cu catalytic electrode at various KOH concentrations.

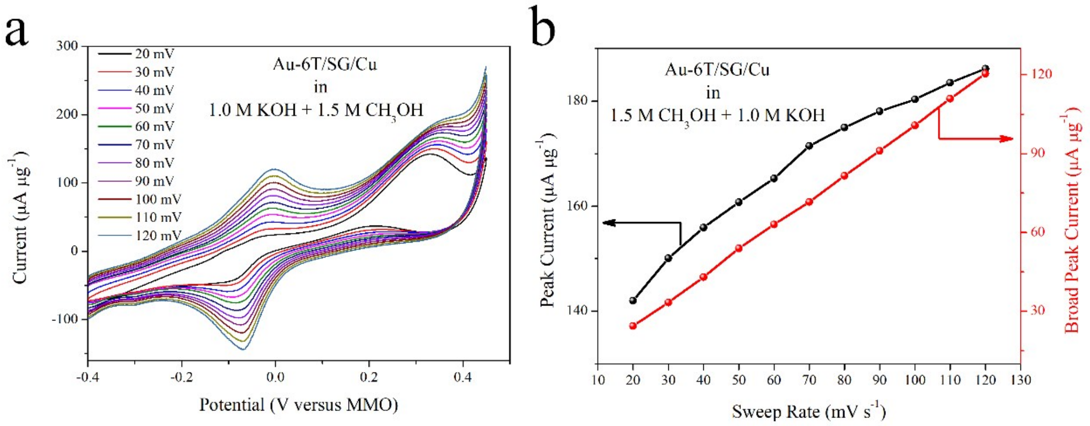

Figure S10 Effect of sweep rate on the methanol oxidation performance of Au–6T/SG/Cu catalytic electrode in a deoxygenated solution of 1.0 M KOH and 1.5 M CH_3OH. (a) CV curves of Au–6T/SG/Cu catalytic electrode recorded at various sweep rates. (b) Anodic peak currents for MOR and broad peak currents for OH^- chemisorption during methanol oxidation on Au–6T/SG/Cu catalytic electrode at various sweep rates.

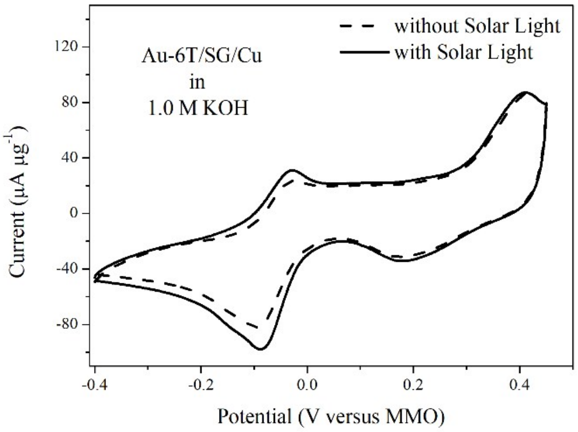

Figure S11 CV curves of Au–6T/SG/Cu catalytic electrode recorded in a deoxygenated solution of 1.0 M KOH in the presence and absence of simulated solar light irradiation.

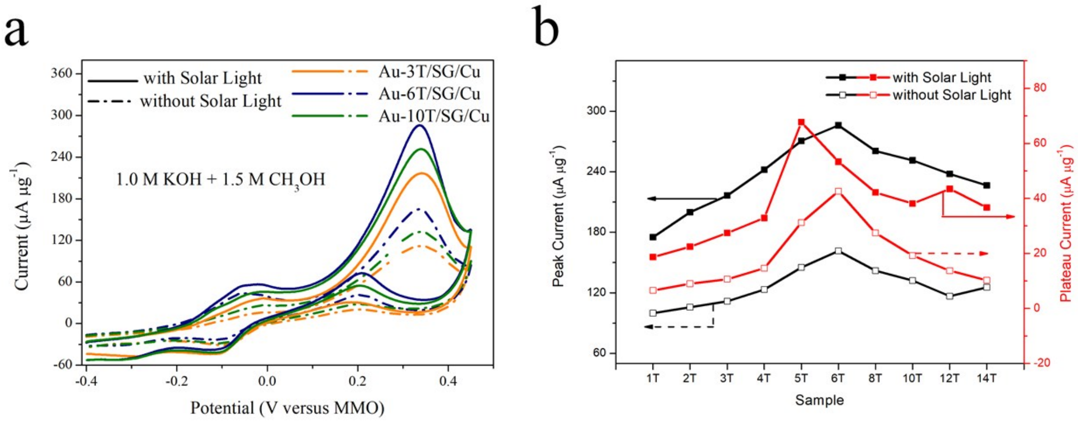

Figure S12 (a) CV curves of Au–3T/SG/Cu, Au–6T/SG/Cu and Au–10T/SG/Cu catalytic electrodes recorded in a deoxygenated solution of 1.0 M KOH containing 1.5 M CH_3OH under the simulated solar light irradiation or not. (b) Anodic peak currents for MOR and OH^- chemisorption during the methanol oxidation on Au–n/SG/Cu (n = 1T–14T) catalytic electrodes in the presence and absence of simulated solar light irradiation.

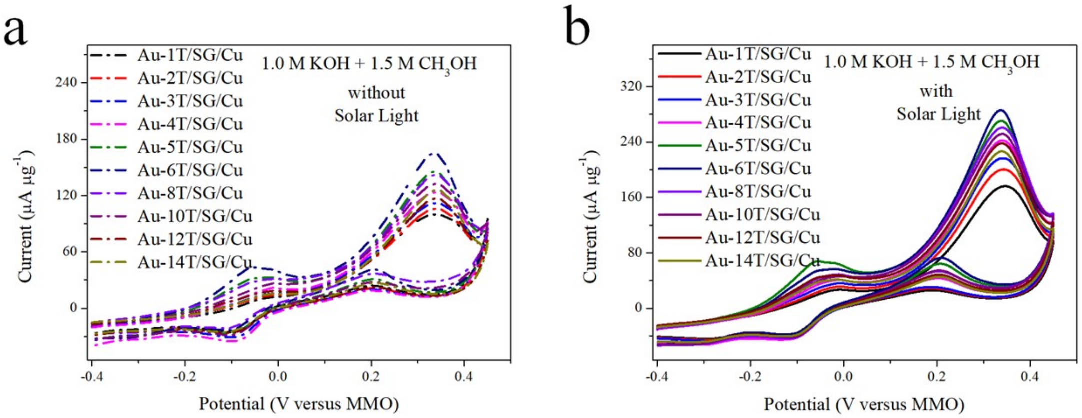

Figure S13 Effect of simulated solar irradiation on the methanol oxidation reaction of various Au–n/SG/Cu catalytic electrodes (n = 1T, 2T, 3T, 4T, 5T, 6T, 8T, 10T, 12T, 14T) in a deoxygenated solution of 1.0 M KOH and 1.5 M CH$_3$OH. CV curves recorded in the (a) absence and (b) presence of simulated solar irradiation.

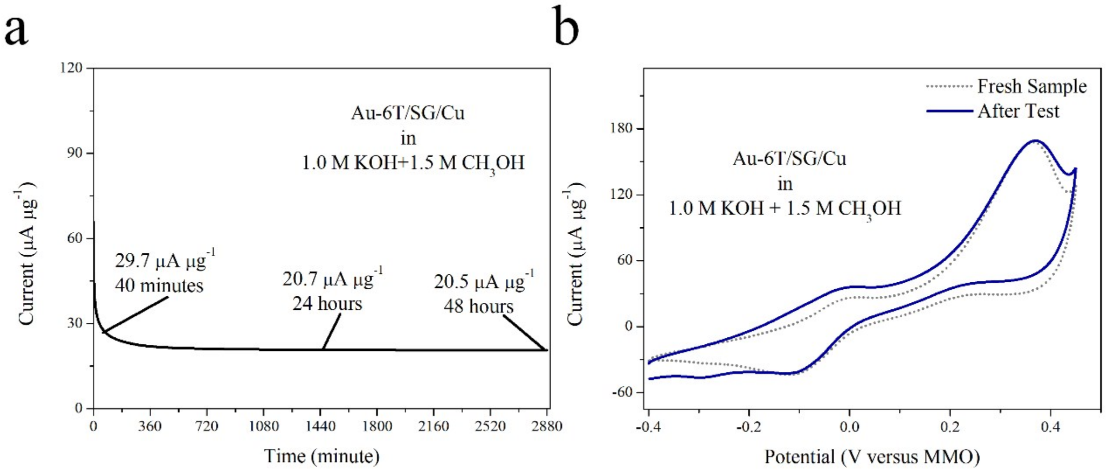

Figure S14 (a) Chronoamperogram of the Au–6T/SG/Cu at the potential of methanol oxidation (0.31 V) in a deoxygenated solution of 1.0 M KOH containing 1.5 M CH_3OH for 48 hours. (b) CV curves of Au–6T/SG/Cu catalytic electrode recorded in a deoxygenated solution of 1.0 M KOH containing 1.5 M CH_3OH before and after the long-term stability test.

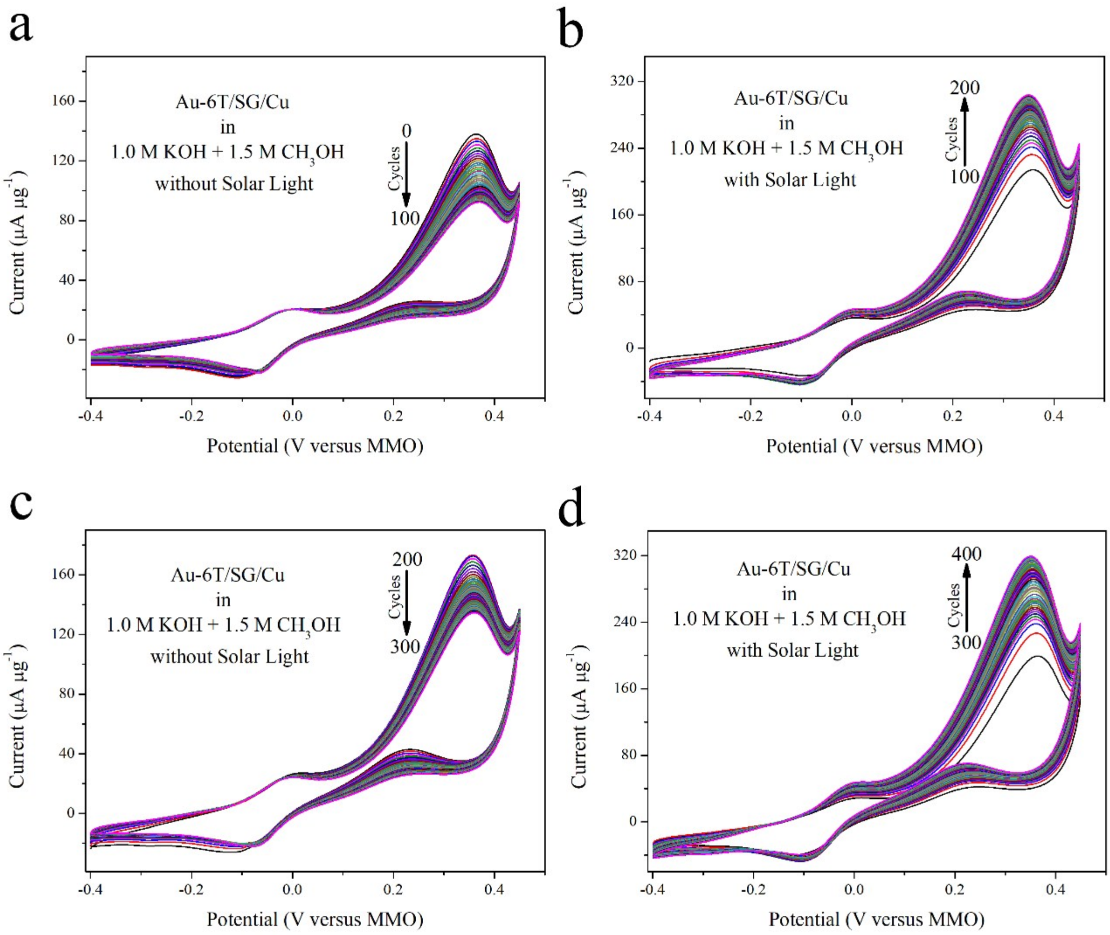

Figure S15 CV curves of Au–6T/SG/Cu catalytic electrode recorded in a deoxygenated solution of 1.0 M KOH containing 1.5 M CH_3OH in the (a, c) absence and (b, d) presence of simulated solar light irradiation.

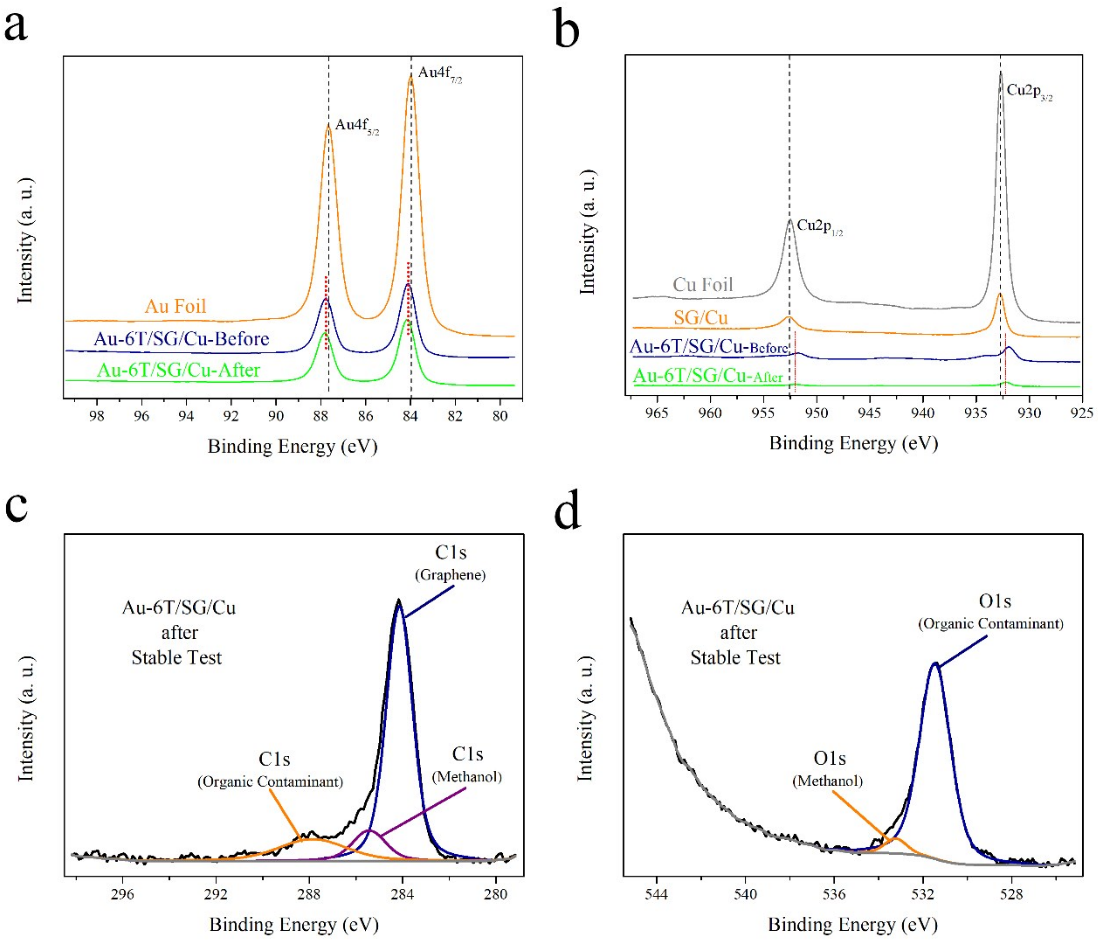

Figure S16 HR-XPS spectra of (a) Au 4f and (b) Cu 2p in the Au–6T/SG/Cu catalytic electrode before and after electrochemical tests and the comparable sample of Au foil, Cu foil, SG/Cu. HR-XPS spectra of (c) C 1s and (d) O 1s in the Au–6T/SG/Cu catalytic electrode after the electrochemical tests.

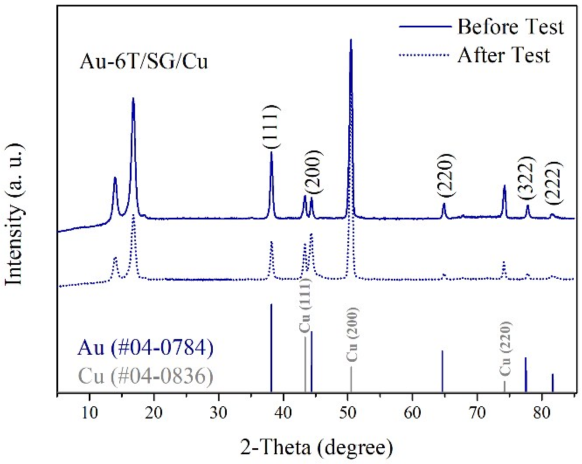

Figure S17 XRD patterns of Au–6T/SG/Cu catalytic electrode catalytic electrode before and after the electrochemical test. The diffraction peaks location for crystalline Au and Cu were confirmed by the JCPDS No. 04-0784 and 04-0836, respectively.

Notes and references

1. C. Wang, X. G. Nie, Y. Shi, Y. Zhou, J. J. Xu, X. H. Xia and H. Y. Chen, *ACS nano*, 2017, **11**, 5897-5905.
2. C. T. Lin, M. N. Chang, H. J. Huang, C. H. Chen, R. J. Sun, B. H. Liao, Y. F. C. Chau, C. N. Hsiao, M. H. Shiao and F. G. Tseng, *Electrochim Acta*, 2016, **192**, 15-21.
3. Z. Jin, Q. Wang, W. Zheng and X. Cui, *Acs Appl Mater Inter*, 2016, **8**, 5273.
4. Y. Liu, F. Chen, Q. Wang, J. Wang, J. Wang and T. T. Gebremariam, *J Mater Chem A*, 2018, **6**, 10515-10524.
5. M. Zhao, H. Xu, S. Ouyang, H. Tong, H. Chen, Y. Li, L. Song and J. Ye, *Acs Catal*, 2018, **8**, 4266-4277.
6. P. Santhosh, A. Gopalan and K. P. Lee, *J Catal*, 2006, **238**, 177-185.
7. S. H. Yan, S. C. Zhang, Y. Lin and G. R. Liu, *J Phys Chem C*, 2011, **115**, 6986-6993.
8. X. X. Yin, N. L. Teradal and R. Jelinek, *Chemistryselect*, 2017, **2**, 10960-10960.
9. S. Pedireddy, H. K. Lee, W. T. Weng, I. Y. Phang, R. T. Hui, Q. C. Shu, C. Troadec and Y. L. Xing, *Nature Communications*, 2014, **5**, 4947.
10. Y. Choi, M. Gu, J. Park, H. K. Song and B. S. Kim, *Adv Energy Mater*, 2012, **2**, 1510-1518.